

The puzzle of metallicity and multiple stellar populations in the Globular Clusters in Fornax

F. D’Antona¹, V. Caloi², A. D’Ercole³, M. Tailo^{4,1}, E. Vesperini⁵, P. Ventura¹,
& M. Di Criscienzo^{6,1} *

¹ *INAF, Osservatorio Astronomico di Roma, Via Frascati 33, I-00040 Monteporzio Catone (Roma), Italy.*

² *INAF, IAPS, Roma, via Fosso del Cavaliere 100, I-00133 Roma, Italy*

³ *INAF- Osservatorio Astronomico di Bologna, via Ranzani 1, I-40127 BOLOGNA (Italy)*

⁴ *Department of Physics, Università di Roma “La Sapienza”, Roma, Italy*

⁵ *Department of Astronomy, Indiana University, Swain West, 727 E. 3rd Street, IN 47405 Bloomington (USA)*

⁶ *INAF, Osservatorio Astronomico di Capodimonte, Via Moiarello 16, I-80131 Napoli (Italy)*

Accepted ... Received ...; in original form ...

ABSTRACT

All models for the formation of multiple populations in globular clusters (GCs) imply an initial mass of the systems several times larger than the present mass.

A recent study of the dwarf spheroidal galaxy Fornax, where the low metallicity ($[\text{Fe}/\text{H}] \lesssim -2$) stars contained in GCs appear to be $\sim 20\%$ of the total, seems to constrain the initial mass of the four low metallicity GCs in Fornax to be at most a factor of 5–6 larger than their present mass.

We examine the photometric data for Fornax clusters, focussing our attention on their horizontal branch (HB) color distribution and, when available, on the RR Lyr variables fraction and period distribution. Based on our understanding of the HB morphology in terms of varying helium content (and red giants mass loss rate) in the context of multiple stellar generations, we show that clusters F2, F3 and F5 must contain substantial fractions of second generation stars ($\sim 54 - 65\%$). On the basis of a simple chemical evolution model we show that the helium distribution in these clusters can be reproduced by models with cluster initial masses ranging from values equal to ~ 4 to ~ 10 times larger than the current masses. Models with a very short second generation star formation episode can also reproduce the observed helium distribution but require larger initial masses up to about twenty times the current mass.

While the lower limit of this range of possible initial GC masses is consistent with those suggested by the observations of the low metallicity field stars, we also discuss the possibility that the metallicity scale of field stars (based on CaII triplet spectroscopy) and the metallicities derived for the clusters in Fornax may not be consistent with each other. In this case, observational constraints would allow larger initial cluster masses.

The reproduction of the HB morphology in F2, F3, F5 requires two interesting hypotheses: 1) the first generation HB stars lie all at “red” colours: namely, they populate only the RR Lyr and the red HB region. According to this interpretation, the low metallicity stars in the field of Fornax, populating the HB at colours bluer than the blue side $-(V-I)_0 \lesssim 0.3$ or $(B-V)_0 \lesssim 0.2$ — of the RR Lyrs, should be second generation stars born in the clusters; a preliminary analysis of available colour surveys of Fornax field provides a fraction $\sim 20\%$ of blue HB stars, in the low metallicity range; 2) the mass loss from individual second generation red giants is a few percent of a solar mass larger than the mass loss from first generation stars.

Key words: stars: horizontal branch; stars: mass-loss; stars: evolution; globular clusters: general; galaxies: dwarf

* E-mail: franca.dantona@gmail.com (FD)

1 INTRODUCTION

The Fornax dwarf spheroidal galaxy (dSph) harbours 5 globular clusters (GCs) (Hodge 1961), having masses, color magnitude diagrams and ages similar to those of Galactic GCs (Buonanno et al. 1998). High dispersion spectroscopy of individual stars in these clusters (Letarte et al. 2006) have recently shown that their stars have abundance anomalies (oxygen, sodium and magnesium spreads) resembling those found in Galactic GCs. These anomalies are the same that provided the initial evidence of multiple stellar populations in Galactic GCs.

Fornax has a high GC specific frequency S_N , defined as the number of GCs normalized to a host galaxy having $M_V = -15$ mag (Harris & van den Bergh 1981): $S_N = 26$ (Larsen et al. 2012a), to be compared with the value $S_N \simeq 1$ typical for spiral galaxies. This specific frequency problem is even more evident if related to the different stellar populations in galaxies, as S_N tends to increase with decreasing metallicity within galaxies (Harris & Harris 2002; Harris et al. 2007), and this holds also for our own Galaxy. The large fraction of Galactic GCs belonging to the halo constitutes a few percent of the halo mass, that indeed, at least in part, could be accounted for by disruption of GCs and loss of stars from them over a Hubble time. The problem of which fraction of the Galactic halo is made up by former GC stars has been emphasized again very recently, in the light of the models for the formation of multiple populations in GCs (Vesperini et al. 2010; Schaerer & Charbonnel 2011). Evidence is accumulating that the majority of stars in GCs belongs to the “second generation” (SG), that turns out to be >50–80% of stars for all clusters examined (Carretta et al. 2009a; D’Antona & Caloi 2008). The main signature of this population, typical of GCs only (Gratton et al. 2012), is the Na-O anticorrelation. The small fraction ($\sim 2.5\%$) of Na-rich and/or CN-rich stars in the field halo (Carretta et al. 2010a; Martell & Grebel 2010) may well come from SG stars evaporated from GCs. All the models for the formation of the SG (both in the asymptotic-giant branch—AGB—scenario and in the rapidly rotating massive stars scenario) need that a great fraction of the first generation (FG) stars is lost from the clusters, in order to account for the present high percentage of SG stars. According to the specific choices for the parameters involved in the models, the ratio between initial mass of the FG and the present mass of GCs harbouring multiple populations must be in the range ≈ 5 –20 (Bekki et al. 2007; D’Ercole et al. 2008; Decressin et al. 2007; Renzini 2008; Carretta et al. 2009a; Bekki 2011), and even up to 100 (Renzini 2013).

The dynamical model by D’Ercole et al. (2008), based on the formation of a SG from the ejecta of massive AGB stars and super-AGB stars, is taken as a basis by Vesperini et al. (2010) to determine the relationship between the fraction of cluster SG stars that are now in the halo and the general contribution of GC stars to the halo. Specifically, Vesperini et al. (2010) showed that the observed fraction of SG stars in the halo (2.5 %) implies that a fraction of about 20%–40% of the halo is composed of stars formed in GCs (if a Kroupa 2001 IMF is assumed; the range is 30 % – 60 % if a Kroupa et al. 1993 IMF is instead adopted; see Vesperini et al. 2010 for further details).

Therefore, models for the formation and evolution of

multiple populations can shed light on the possible contribution of GCs to the halo assembly and seem to suggest that stars originally formed in GCs are a significant fraction of the Galactic halo. Even more so, exploring the connection between multiple populations and the field population of dSph galaxies with a high specific frequency of GCs can provide additional insight and constraints on the formation and dynamical history of GCs. Larsen et al. (2012a) compared the low-metallicity GC populations in Fornax with the corresponding field star population and concluded that the initial mass of these clusters can not have been larger than a factor ~ 5 their present mass. Moreover, in the same range of metallicity, there can not have been other clusters now dissolved in the field.

In this paper we estimate the fraction and the distribution of helium content of SG stars in the low metallicity GCs in Fornax following the analysis of the HB morphology described by D’Antona et al. (2002). On this basis, we present a set of simple chemical models aimed at constraining the range of initial masses of GCs. We review the possible problems in the metallicity scales of GCs and field stars, and summarize how these uncertainties might affect the observational constraints on the GC initial mass.

2 MODELS FOR THE FORMATION OF FORNAX CLUSTERS

2.1 Stellar evolution and synthetic horizontal branch computation

We computed one basic set of isochrones and HB evolutions for this work. We adopt the metallicity $Z = 0.0003$, and consider three helium contents, in mass fraction $Y = 0.25, 0.28$ and 0.35 . For an α -enhancement $[\alpha/\text{Fe}] = 0.4$, with a choice of $Z_\odot = 0.018$, this corresponds to $[\text{Fe}/\text{H}] \sim -2$, appropriate for several low metallicity Galactic GCs, although formally too large to describe the clusters F1, F2, F3 and F5 in Fornax (but see Section 3). For $T > 10000$ K we used the OPAL opacities, in the version documented by Iglesias & Rogers (1996), with all the recent updates; at lower temperatures the opacities by Ferguson et al. (2005) were adopted. Conductive opacities were taken from the WEB site of Potekhin (year 2006)¹, corresponding to Potekhin et al. (1999) treatment, corrected following the improvement of the treatment of the e–e scattering contribution described in Cassisi et al. (2007). Other inputs (convection model, non instantaneous mixing, treatment of the borders of convection) are all as described e.g. in Di Criscienzo et al. (2011). We followed the main sequence and red giant (RG) evolution of low mass tracks. We compute isochrones from 9 to 14 Gyr for the chosen chemistry and the helium core mass at the helium flash. The RG evolution was followed at constant mass. The core masses are taken as input for the computation of HB models; the small helium increase in the envelope during the evolution is also taken into account.

Synthetic models for the HB are computed according to the recipes described in D’Antona & Caloi (2008). We adopt the appropriate relation between the mass of the evolving giant M_{RG} and the age, as function of Y . The mass on the

¹ see <http://www.ioffe.rssi.ru/astro/conduct>

HB, as assumed in our previous work of HB simulations, is then simply:

$$M_{HB} = M_{RG}(Y, Z) - \Delta M \quad (1)$$

ΔM is the mass lost during the RG phase. We assume that ΔM has a gaussian dispersion σ around an average value ΔM_0 and that both ΔM_0 and σ are parameters to be determined and *in principle* do not depend on Y . We will see that a reasonable fit of the morphology of the Fornax clusters HBs requires that *the mass loss of the second generation stars is larger than in the FG stars*, by a small but significant amount. We then modify the expression to:

$$M_{HB} = M_{RG}(Y, Z) - \Delta M - \delta M_{SG} \quad (2)$$

so that ΔM is fixed for both populations in order to fit the redder HB stars that we attribute to the FG, and δM_{SG} will be fixed, along with a number vs. helium distribution assumed for the SG, in order to satisfactorily reproduce the bluer parts of the HB. For given values of Z and Y , the T_{eff} location of an HB mass is fixed. Consequently, different ages can be adopted, provided that the mass loss is consistently adjusted. The RR Lyr variables are identified as those stars that, in the simulation, belong to the T_{eff} interval $3.795 < \log T_{\text{eff}} < 3.86$. Their periods are computed as in Di Criscienzo et al. (2004, see their Eq. 1).

2.2 Chemical evolution models

Once acquired the helium distribution function $N(Y)$ that best accounts for the star distribution along the cluster HB, we attempt to reproduce it by means of D’Ercole et al. (2010, 2012) chemical evolution model, hereafter referred to as D2010 and D2012. According to the framework presented in D2010, FG stars are already in place and have the same chemical abundances of the pristine gas from which they form; the SG stars form from super-AGB and AGB ejecta collecting in the cluster centre through a cooling flow, partially diluted with pristine gas also accreting in the cluster core. For the Fornax clusters, we have adopted the yields from the latest computations by Ventura et al. (2013), that refer to the global metallicity $Z=0.0003$ (as specified above). There are not enough spectroscopic data to test the results of our models on other elements abundances (e.g. oxygen and sodium abundances), and here we focus only on the Y distribution, $N(Y)$. The chemical evolution models consistent with the $N(Y)$ derived from the HB observations will provide the ratio of the SG to the clusters initial masses (see Section 5).

3 THE METALLICITY OF GCS AND FIELD STARS

3.1 The metal-poor component in the Fornax field and CaII triplet calibration

In the last twenty years CaII triplet spectroscopy applied to GC red giants has been frequently used as a proxy for Fe-abundance (e.g. Da Costa & Armandroff 1995; Rutledge et al. 1997; Da Costa & Hatzidimitriou 1998). The method has been extended to intermediate age clusters and field stars of various age and composition in nearby

Galactic satellites (e.g., Tolstoy et al. 2001; Cole et al. 2004). The advantages and the drawbacks of the method are discussed in detail in those papers and references therein. As pointed out, among others, by Da Costa & Hatzidimitriou (1998), the theoretical basis of the method is not well understood, since the dependence of the intensity of the CaII triplet on Ca- and Fe- abundances is not known. Besides, the method is calibrated on GC giants, where $[\text{Ca}/\text{Fe}]$ is assumed to be about +0.3; if used for giants with lower values of $[\text{Ca}/\text{Fe}]$, it will lead to an underestimate of $[\text{Fe}/\text{H}]$. Another important point is the choice of the abundance scale for GCs, which of course will influence the Ca-triplet calibration.

In the case of Fornax field, the situation is discussed in detail by Tolstoy et al. (2001), Battaglia et al. (2006, 2008) and Starkenburg et al. (2010). Tolstoy et al. note that the abundances of individual stars do not always correspond to their colour, an occurrence to be kept in mind when considering the possible loopholes of the method. At the same time, Battaglia et al. (2008) and Starkenburg et al. (2010) propose the ultimate solution of the problem, with a direct calibration of the Ca-triplet through high resolution spectroscopy of 36 giants in the Fornax field. The latter paper extends the relation found in the former down to a very low Fe-content $[\text{Fe}/\text{H}] \simeq -4$ dex. In this Fe-abundance range the errors increase, but not to the point of affecting the estimate of an extreme Fe-deficiency (Starkenburg et al. 2010, Fig. 10).

As a matter of fact, the sample of high resolution observations in Battaglia et al. (2008) consists of 36 RG stars, for 33 of which the estimated $[\text{Fe}/\text{H}]$ is ≥ -1.0 , while for the remaining three we have $[\text{Fe}/\text{H}] = -1.44, -1.53$ and -2.65 . Besides, the estimates for these three stars through the adopted CaII calibration, based on Carretta & Gratton scale (1997), are $[\text{Fe}/\text{H}] = -1.81, -1.85, -2.39$, values significantly different from those derived through high resolution spectroscopy. Therefore we consider difficult to establish a reliable calibration of the low metallicity tail in Fornax field on this basis. There is another important point: recently, the Carretta & Gratton scale has been substantially changed (Carretta et al. 2009b). According to the authors, among the main reasons behind this result are: the adopted temperature scale and the difference in the gf -values. In any case, the CaII triplet calibrations should be reconsidered. We observe also that the extreme sensitivity of high resolution spectroscopy on the adopted parameters for spectra interpretation is still not under control and should suggest caution in the estimates of the errors involved.

An interesting point is raised by Starkenburg et al. (2010): Fornax exhibits a low-metallicity tail much less pronounced than in many other dwarf spheroidals and ultra-faint galaxies (see their Fig.14). They wonder whether this fact is due to a different chemical history in the early epochs, or if the low metallicity population is being hidden by the dominant young and metal-rich population (this would be possible since the observed sample in Fornax is a very small fraction of the total number of RG stars in this galaxy).

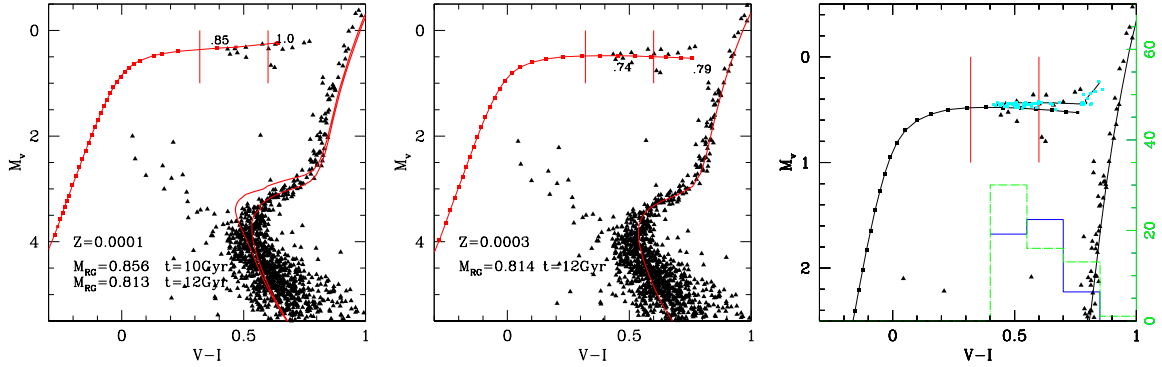


Figure 1. The color magnitude diagram of cluster F1 from Buonanno et al. 1998 is shown. In the left panel, the data have been reported to absolute magnitude and intrinsic colour by assuming a reddening $E(V-I)=0.02$ and a distance modulus $(V-M_v)=20.85$; the choice has been made to allow for a match with the ZAHB location of models with $Z=10^{-4}$. Along the ZAHB, the positions of 0.85 and 1.0 M_{\odot} are indicated; the isochrones and corresponding RGB mass for ages 10 and 12Gyr are given. We see that an age of 10Gyr is barely compatible with the HB data, while the relative morphology of HB and turnoff are not. In the central panel, we show the same data, assuming the same dereddening and $(V-M_v)=20.75$, to compare with ZAHB and isochrones for $Z=3 \times 10^{-4}$. We see that for this Z there is ample space in the mass loss in order to reproduce the HB. In the right panel, we show a simple simulation of the HB data, obtained with a unique population of FG stars at $Y=0.25$, $Z=3 \times 10^{-4}$. At the bottom, we show the histogram of the number of HB stars versus $V-I$ (full line) compared with the histogram of the simulation (dashed).

3.2 The determination of $[\text{Fe}/\text{H}]$ in Fornax clusters

The precise metallicity of Fornax clusters is a key element for our analysis. Strader et al. (2003) collect and discuss their $[\text{Fe}/\text{H}]$ estimates along with those preceding their work. These estimates are based on low resolution spectra, various photometric indices and CM diagram features, and give values never lower than -2.1 dex. Recently, high resolution spectroscopy of both individual stars and integrated cluster light have given much lower values of $[\text{Fe}/\text{H}]$ for F1, F2, F3 and F5. For example, Larsen et al. (2012b) obtain $[\text{Fe}/\text{H}] = -2.35$ for F3 through the analysis of integrated cluster spectra. The spectra are interpreted by means of synthetic population analysis based on stellar counts (from the photometric data by Buonanno et al. 1998), extrapolated to lower luminosity by appropriate isochrones (Dotter et al. 2007). They say that this value agrees “reassuringly well” with the value of $[\text{Fe}/\text{H}] = -2.4 \pm 0.1$ derived by Letarte et al. (2006) from high dispersion spectroscopy of three stars in F3. As mentioned before, this is significantly lower than both the old value listed by Buonanno et al. (1998) of -1.96 ± 0.20 , based on the slope of the RG branch, and the more recent one of -1.84 ± 0.18 given by Strader et al. (2003) on the basis of low-resolution integrated spectra. Another estimate comes from Greco (2007), who find $[\text{Fe}/\text{H}] = -1.91$ from the mean period of ab-type RR Lyrs, using Sandage (1993) relation. Similar considerations hold as well for F2, F5 and F1. For this latter cluster observational data are scarcer, but Letarte et al. (2006) find $[\text{Fe}/\text{H}] = -2.5 \pm 0.1$ (again from high-dispersion spectra of three members), significantly lower than the values listed by Strader et al. (2003).

Although a review and analysis of existing observations is well beyond the scope of this work, we argue in the following sections that values of $[\text{Fe}/\text{H}]$ lower than ~ -2.2 can be excluded on evolutionary considerations.

3.3 The conversion between $[\text{Fe}/\text{H}]$ and metals mass fraction

The global metallicity, that is the metal mass fraction Z which enters in stellar structure computation, can be derived by choosing the elemental solar ratios of abundances, an appropriate relation between metallicity, $[\text{Fe}/\text{H}]$ and $[\alpha/\text{Fe}]$, and the solar metal abundance. We derived the following two relations: the first one based on the Grevesse & Sauval (1998) (GS98) elemental solar ratios.

$$\log(Z/Z_{\odot}) = [\text{Fe}/\text{H}] + 0.72[\alpha/\text{Fe}] - 0.15[\alpha/\text{Fe}]^2 + \log(X/X_{\odot}) \quad (3)$$

and the second one based on the elemental ratios by Asplund et al. (2009) (AS09):

$$\log(Z/Z_{\odot}) = [\text{Fe}/\text{H}] + 0.69[\alpha/\text{Fe}] - 0.16[\alpha/\text{Fe}]^2 + \log(X/X_{\odot}) \quad (4)$$

The global metallicity Z is obviously dependent also on the solar metallicity Z_{\odot} . The value $(Z/X)_{\odot} \simeq 0.023$ applies to Grevesse & Sauval (1998) determination, and a value $(Z/X)_{\odot} \simeq 0.018^2$ corresponds to Asplund et al. (2009) determination. The downward revision is a result of the analysis of solar spectral lines based on 3D hydrodynamic models of the solar atmosphere, a careful selection of spectral lines, and relaxing the assumption of LTE. Nevertheless, we have to mention the “solar abundance problem” emerged with the new solar abundances. The Grevesse & Sauval (1998) value of $(Z/X)_{\odot}$ allowed the construction of a “standard solar model” perfectly matching the detailed structure of the solar interior that emerged from helioseismic studies (Christensen-Dalsgaard et al. 1996; Bahcall et al. 2001). On the contrary, computation of solar models incorporating reduced CNO abundances (Bahcall et al. 2004; Basu & Antia

² Notice that the ratio $(Z/X)_{\odot}$ is the value observed at the solar photosphere. The action of diffusion in the 4.6 billion years of solar lifetime is such that the hydrogen mass fraction is increased to $X_{\odot} \simeq 0.76$, so that the resulting solar mass fractions are $Z_{\odot} \simeq 0.018$ for GS98, and $Z_{\odot} \simeq 0.014$ for AS09.

Table 1. Conversion $[\text{Fe}/\text{H}] - Z$

[Fe/H]	$Z_{\odot}=0.014$ AS09			$Z_{\odot}=0.018$ GS98		
	$[\alpha/\text{Fe}]=0.1$	$[\alpha/\text{Fe}]=0.2$	$[\alpha/\text{Fe}]=0.4$	$[\alpha/\text{Fe}]=0.1$	$[\alpha/\text{Fe}]=0.2$	$[\alpha/\text{Fe}]=0.4$
-2.5	5.2×10^{-5}	6.0×10^{-5}	7.9×10^{-5}	6.7×10^{-5}	7.8×10^{-5}	9.1×10^{-5}
-2.4	6.5×10^{-5}	7.5×10^{-5}	1.2×10^{-4}	8.4×10^{-5}	9.8×10^{-5}	1.3×10^{-4}
-2.3	8.2×10^{-5}	9.5×10^{-5}	9.9×10^{-5}	1.1×10^{-4}	1.2×10^{-4}	1.7×10^{-4}
-2.2	1.0×10^{-4}	1.2×10^{-4}	1.6×10^{-4}	1.3×10^{-4}	1.6×10^{-4}	2.1×10^{-4}
-2.1	1.3×10^{-4}	1.5×10^{-4}	2.0×10^{-4}	1.7×10^{-4}	2.0×10^{-4}	2.6×10^{-4}
-2.0	1.6×10^{-4}	1.9×10^{-4}	2.5×10^{-4}	2.1×10^{-4}	2.5×10^{-4}	2.9×10^{-4}
-1.5	5.2×10^{-4}	6.0×10^{-4}	7.9×10^{-4}	6.7×10^{-4}	7.8×10^{-4}	1.0×10^{-3}
-1.4	6.5×10^{-4}	7.5×10^{-4}	9.9×10^{-4}	8.4×10^{-4}	9.8×10^{-4}	1.3×10^{-3}

2004; Montalbán et al. 2004) showed that the location of the boundary of the solar convective envelope, the sound speed and density profiles, and today’s surface helium abundance predicted by models using low $(Z/X)_{\odot}$, differ from the values obtained from helioseismology by amounts beyond accepted uncertainties (Bahcall et al. 2006). Models in satisfactory agreement with these data can be built, but they rely on parametric adjustments either of interior opacities, or of other pieces of input physics (Bahcall et al. 2005; Montalbán et al. 2006).

3.4 Problems concerning the metallicity of globular clusters F1 and F4

The question we intend to pose appears very clear when discussing the cluster F1. We shall discuss the maximum possible range of metallicities that correspond to $[\text{Fe}/\text{H}]=-2.5 \pm 0.1$ estimated for F1 by Letarte et al. (2006). For the sake of argument, let us assume $[\alpha/\text{Fe}]=0.2$ (see the estimates of calcium for Fornax clusters in Larsen et al. 2012b).

From the correspondence between $[\text{Fe}/\text{H}]$ and metal mass fraction listed in Table 1, we see that a value of $Z=10^{-4}$ for $[\alpha/\text{Fe}]=0.2$ overestimates the abundances measured by Letarte et al. (2006) in individual cluster stars. We then used the isochrones and horizontal branch models computed for this composition by Di Criscienzo et al. (2011) for comparison with F1 data. The left panel of Fig. 1 shows that an age of 12 Gyr is incompatible with the very red HB of this cluster: in fact, the evolving RGB mass is a bare 0.81 M_{\odot} , while the blue edge of the HB requires a zero age HB value of 0.85 M_{\odot} . Even if no mass is lost along the RGB, the cluster can not be older than ~ 9.5 Gyr. Such a value is in contrast with the relative location of the HB and the turnoff and, besides, Buonanno et al. (1998) showed that the loci of the four clusters F1, F2, F3 and F5 can be superimposed on each other, as well as on the old metal poor GCs M 68 and M 92.

In order to obtain a reasonable fit of F1 CM diagram, we move to isochrones and HB models of $Z=0.0003$ and $[\alpha/\text{Fe}]=0.4$, that clearly overestimate the metallicity and $[\alpha/\text{Fe}]$ of this cluster. In this case, the RGB mass is still 0.81 M_{\odot} at 12 Gyr, but the HB locations at fixed mass have moved to redder colors, thanks to the larger efficiency of the H-burning shell, and we find a value of 0.75 M_{\odot} for the bluest HB objects of F1 (Fig.1, central panel). Therefore, there is enough space between $Z=0.0001$ and $Z=0.0003$ to

achieve a reasonable fit of the CM diagram features of this cluster. While core hydrogen burning and lifetimes do not strongly depend on the metallicity at such low values —and the evolving mass does not change by shifting Z from 1 to 3×10^{-4} — the location in T_{eff} of masses along the HB is in fact linked to the relative efficiency of He-core burning and H-shell burning in the star: by increasing the metallicity, we increase the CNO in the hydrogen shell, and make the shell burning more efficient, so that smaller masses move to lower T_{eff} . In order to locate a mass equal to the evolving RG mass (0.81 M_{\odot} at 12 Gyr) at the bluest location of F1 HB, it is necessary to increase Z to $\sim 1.5 \times 10^{-4}$, that is to $[\text{Fe}/\text{H}] \sim -2.3$ to -2.2 (according to the chosen Z_{\odot}).

The study of the exact composition of F1 stars is beyond the scope of this paper, we only wish to point out that the “formal” metallicity derived from high dispersion spectroscopy is not compatible with cluster features. As for the problem of the formation of this cluster, we also can point out that looks like a “first generation only” cluster, in the sense of Caloi & D’Antona (2011). In fact, the distribution of its HB stars with colour can be interpreted as due to the evolution of masses $M=0.74 \pm 0.005 M_{\odot}$, deriving from a simple stellar population with cosmological Y content aged 12 Gyr that has lost $\sim 0.07 M_{\odot}$ on the RGB. The result is shown in the right panel of Fig.1, with the simulated HB population and the corresponding histogram (dash dotted).

The small current mass of F1 might be consistent with the lack of a SG population (although it is important to point out that the cluster mass and structural properties which are relevant for the SG formation are the initial ones and those might significantly differ from the current ones). In this context, we notice that Letarte et al. (2006) provide abundances for three stars in F1, and find remarkable abundance differences in sodium, oxygen and magnesium. If confirmed, these are not consistent with our interpretation, but the sample is too limited to draw any conclusion.

In this work, we leave aside the discussion of cluster F4; its role is not particularly relevant for the problem of multiple population formation, as its most recent $[\text{Fe}/\text{H}]$ value lies in the range where field stars are very abundant. Nevertheless, it is interesting to point out some issues concerning the metallicity of this cluster.

First of all, the range of $[\text{Fe}/\text{H}]$ attributed to F4 goes from -1.4 to -2.2 (summary Table 5 in Strader et al. (2003)). A value $[\text{Fe}/\text{H}]=-1.4$ is also found by Larsen et al. (2012a). The α -enhancement, if any, is very low, so the global metallicity we can derive from Table 1 is $6-8 \times 10^{-4}$. The reddening

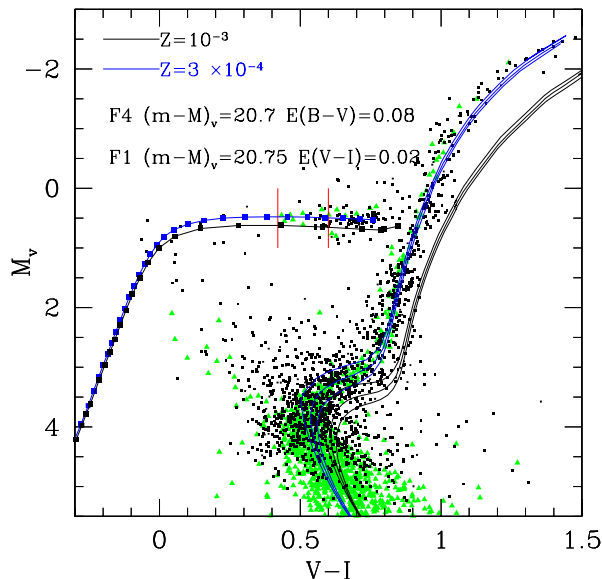


Figure 2. The data for clusters F1 (green triangles, from Buonanno et al. 1998) and F4 (black dots, from Buonanno et al. 2009) are superimposed by assuming for F4 the minimum reddening that allows to populate the RR Lyr strip (Greco et al. 2009) and a distance modulus compatible with the plotted ZAHB locations of the $Z=0.0003$ and $Z=0.001$ models. We also show isochrones of 10, 12 and 14 Gyr for both metallicities (the $Z=0.001$ isochrones are redder). As well documented in Buonanno et al. 2009, we see that the morphology of the RGB and turnoff regions are not compatible with a difference in metallicity of a factor 10 between the two clusters.

ing values $E(B-V)=0.08-0.12$ quoted in the literature are mandatory to place at least the bluest part of its HB stars into the RR Lyr gap (many RR Lyr variables are present in the cluster Greco et al. (2009)). Once applied the lowest reddening $E(B-V)=0.08$ mag, and a distance modulus consistent with the level of the HB, we re-discover the result largely discussed in Buonanno et al. (1999), namely, that the turnoff and RG colours result very similar to the colours of cluster F1 (Fig. 2). Also the RGB slopes are similar, a finding that led Buonanno et al. (1999) to propose an $[Fe/H] \simeq -2$ for this cluster. We remark that it is difficult to believe in a metallicity difference of 1.1 dex (from -2.5 for F1 to -1.4 for F4) as proposed in the recent determinations.

One can suggest that the information that the HB stars occupy only the RR Lyr region and the red HB is in favor of a larger average metallicity, but we have seen that the HB of F1 is red too, and will discuss in Sect. 4 that we expect not very blue HBs for the FG of the other clusters. As the HB of F4 is not very extended in color, we are led to interpret it as a FG-only population. This is however in contrast with the relatively large mass of the cluster, and especially with its concentration. Further effort is necessary to understand the precise role of star formation in this cluster.

4 THE EXTENT OF THE SG IN CLUSTERS F2, F3 AND F5

At first sight, the CM diagrams of clusters F2, F3 and F5 (Buonanno et al. 1998) may be misleading. Cluster F2 has a “short” blue HB, that could resemble the luminous part of the very extended HB of NGC 2419, interpreted by Di Criscienzo et al. (2011) as the FG fraction of the cluster stars. The RR Lyrs in NGC 2419 are not on the zero age HB, but lie on tracks starting on the blue HB: however, their luminosity is close to the zero age luminosity (as appropriate for very metal poor evolutionary tracks). The HB in F5 looks like that in F2, but it has a short blue extension, so we could be led to think that this extension represents a small SG with a slightly increased helium content (like in the cluster M 53, in the simulations by Caloi & D’Antona 2011). Only F3 has a very extended HB that resembles a cluster with a high percentage of SG. If this were the case, the problem of the small fraction of stars having the clusters metallicity in Fornax field would be simple to solve, as there is only one cluster, F3, with a second generation that requires a strong FG mass loss during the early phases of this cluster dynamical evolution.

A closer look at the HBs, however, shows that this is not the case, and that all the three cluster have a large fraction of SG stars. We examine them in order of increasing colour extent of their HB.

4.1 Simulations of the HB in F2

In F2, Letarte et al. (2006) find $[Fe/H]=-2.1 \pm 0.1$ from high dispersion spectra. We use our evolutionary tracks for $Z=0.0003$ and standard helium content $Y=0.25$ to describe the FG of this cluster. The distance modulus and reddening are chosen, within reasonable values, to fit our own models. For this cluster we adopt $(V-M_v)=20.88$ and $E(V-I)/E(B-V)=0.05$. We use a ratio $E(V-I)/E(B-V)=1.3$, and an absorption $A_v=3.1E(B-V)$. We first attempt an “FG only” description of the HB. The left panel of Fig. 3 shows the result. The age chosen for the cluster is a standard 12Gyr, the mass loss on the RGB had to be fixed at $\Delta M=0.13M_\odot$, to fit the bluer end of the HB, and a mass dispersion $\sigma=0.015M_\odot$ has been chosen to spread the HB as required (model 2 in Table 2). The evolving masses have a peak in the range $0.68-0.69M_\odot$. Nevertheless, it is well clear that the number of stars in the RR Lyr region *where the colour distribution shows a secondary maximum* can not be reproduced, as the models spend most of their lifetime in the blue, and evolve fastly at the RR Lyr location. The total number of HB stars is 120, but the total number of simulation stars shown is 850, and the histogram plots the number in each bin divided by 10, corresponding to a total of 85 stars. With such a choice, we normalize the simulation to the number counts in the bins at the left of the RR Lyr gap³ From this comparison, we see that the star distribution along the HB is very different from the distribution in the luminous part of the HB of

³ If we normalize to the total number of observed stars (120), the comparison amplifies the inconsistency between the color distribution of the data set and that of the simulation, as most of the extra stars would raise the number at the blue HB side, while the red side would still show fewer stars than observed.

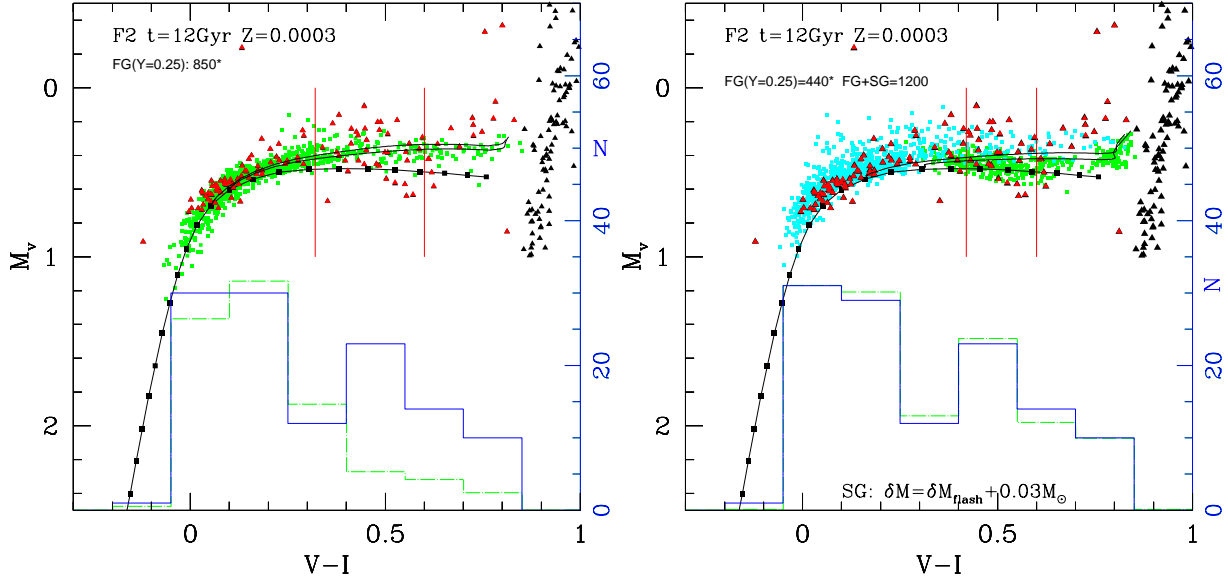


Figure 3. The panels show the HST data in the bands F555 (labelled V) and F814 (labelled I) for the cluster F2, from Buonanno et al. 1998 (red and black triangles). The full line connecting the black squares represents the ZAHB for the models of $Z=0.0003$ and $Y=0.25$. Two HB tracks are shown, for $M=0.68$ and $0.69M_{\odot}$ in the left panel, for $M=0.70$ and $0.72M_{\odot}$ in the right panel. The RR Lyr gap is approximately limited by the vertical red lines. Red triangles indicate the stars we consider as HB members (120), for which the full line histogram at the bottom shows the number vs. colour distribution. The simulations are shown by green squares (FG) and cyan squares (SG): see text for details. The corresponding colour distributions are shown in both panels as dot-dashed histograms. The left panel shows the HB data for F2, together with an attempt of simulating them by means of a unique FG population (model 2 in Table 2): RR Lyrs and red HB stars are not accounted for. The right panel shows the comparison with simulation model 4, able to reproduce the peak of stars in the RR Lyr region. This assumes the presence of a SG population having larger helium abundances and larger mass loss on the RGB, by $0.03M_{\odot}$.

Table 2. Simulations parameters

	Cluster	Z	age(Gyr)	$\delta M_{RG-HB}/M_{\odot}$	$\delta M_{RGadd.}/M_{\odot}$	$\sigma(M_{\odot})$	N_{SG}/N_{tot}
1	F1	0.0003	12	0.069	0	0.012	0
2	F2	0.0003	12	0.13	0	0.015	0
3	F5	0.0003	12	0.130	0	0.015	40
4	F2	0.0003	12	0.0735	0.03	0.004	58
5	F3	0.0003	12	0.0713	0.03	0.009	54
6	F5	0.0003	12	0.0770	0.03	0.008	65

NGC 2419: in the latter cluster the peak in the blue is much more pronounced; besides, the RR Lyr and red HB stars can not be ascribed to the evolved part of the HB tracks starting in the blue HB peak.

In order to fit the HB of this cluster, it is necessary to reduce the mass loss along the RGB for the FG, and to reproduce the peak in the RR Lyr gap *as the locus of evolution of the FG stars* (see the simulations for M 3 in Caloi & D’Antona 2005). The successful simulation parameter are those of model 4 in Table 2. In order to reproduce the bluer parts of the HB, we attribute them to a SG, with increasing values of the helium content for increasing T_{eff} (right panel of Fig.3). To obtain a satisfactory fit to the observed HB morphology in the colour-magnitude diagram, we had also to add a $\delta M_{SG}=0.03M_{\odot}$ to the mass loss of the SG. We will discuss the necessity of this choice in Sect. 6.1.

As a result, the FG population in this cluster, obtained from the HB morphology, is 42% of the total.

4.2 Simulations of the HB in F5

Also for F5, listed at $[\text{Fe}/\text{H}]=-2.1$ by Larsen et al. (2012b), we use the $Z=0.0003$ composition. We adopt $(V-M_v)=21.0$ and $E(V-I)=0.05$. The left panel of Fig. 4 shows the result of the simulation model 3, in which we attempt to reproduce the HB by assuming a FG starting its HB evolution at $V-I \simeq 0$; a larger helium content is assumed for a SG reproducing only the bluer and fainter stars. The FG percentage for this choice is 60%. The simulation, however, fails to reproduce the numerous RR Lyr stars, and the red side of the HB, as in F2. We then resort to a reduced mass loss on the RGB ($0.077M_{\odot}$), so to reproduce the peak in the

RR Lyrs by the evolution of the FG stars in their longest burning phase, and adopt larger helium content (SG signature) for all the stars bluer than $(V-I)_0 \sim 0.3$ (Fig.4, central panel). The percentage of FG stars is then reduced from 60% of the first simulation to only 35%. The distribution obtained for the RR Lyr periods is compared with the data by Greco et al. (2009) in the right panel of Fig.4. This simulation has been performed by adopting the same number of HB stars as available in the sample, and the total number of RR Lyrs obtained is ~ 30 , like in the observations. If the distribution of periods is obtained by adopting ten times more stars (as in the simulation shown in the central panel), there appears a tight peak in the period distribution, similar to what we see in the cluster M3, where the number of RR Lyr is very large (about 200, see Caloi & D’Antona 2008).

4.3 Simulation of the HB in F3

Larsen et al. (2012b) assign $[\text{Fe}/\text{H}] = -2.3 \pm 0.1$ to this cluster. The metallicity corresponding to $[\text{Fe}/\text{H}] = -2.3$ is $Z = 0.95 - 1.2 \times 10^{-4}$ for $[\alpha/\text{Fe}] = 0.2$, or $Z = 1 - 1.7 \times 10^{-4}$ for $[\alpha/\text{Fe}] = 0.4$. The case $Z \sim 10^{-4}$ is to be excluded for the reasons discussed in Sect.3.4, since the colour distribution of HB stars has a local maximum in the RR Lyr region, like in F2 and F5; a value in the upper range (e.g. $Z = 1.5 \times 10^{-4}$) would allow a meaningful simulation. Also for this cluster we adopt models with $Z = 0.0003$, as we are mainly interested in the percentage of SG stars, and this is scarcely dependent on the exact metallicity.

Figure 5 shows one satisfactory simulation (model 5 in Table 2). For an age of 12Gyr, we have set $\Delta M = 0.0713 M_\odot$ to locate most of the FG in the RR Lyr region, and we have added several SG samples, with increasing helium up to $Y = 0.34$, in order to account for the blue part of the HB that extends to T_{eff} larger than for the other clusters. The percentage of FG stars is here $\sim 46\%$. One may wonder why the cluster with the largest extension of the HB has in fact a slightly smaller percentage of SG. The main difference with the cases of F2 and F5 is the following: in F3, although we have also to account for a fraction of stars with more extreme colors, the most prominent number of stars in the HB is at the RR Lyr colour location, occupied mainly by the FG. Notice that the simulation shows also SG (evolved) stars in the RR Lyr region: this should be reflected in their period distribution, that is not yet available. Finally, notice that again we had to add a $\delta M_{\text{SG}} = 0.03 M_\odot$ to the mass lost in the RGB evolution by SG stars.

5 APPLICATION OF THE CHEMICAL EVOLUTION MODEL AND THE INITIAL MASS OF F2, F3 AND F5

In order to obtain a guess on the initial (pure FG) mass of the clusters, we resort to our chemical evolution model described in D2010. This is a one-zone model in which the interstellar gas (ISM) is supposed to be initially absent owing to the clearing action of the FG Type II supernovae explosions; the ISM is successively supplied by the FG AGB ejecta and by the accretion of pristine gas, and is depleted by the SG star formation. The model is characterized by the initial FG density $\rho_{*,\text{FG}}$ and by a gaussian temporal profile

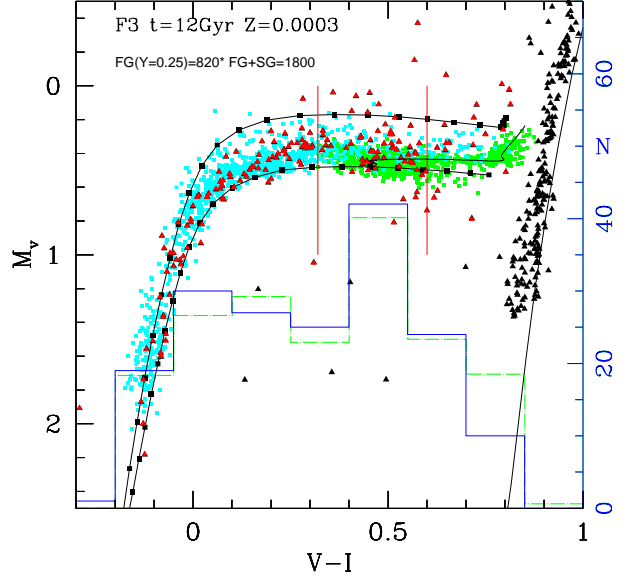


Figure 5. The result for F3 of simulation 5 in Table 2. The red triangles represent the observed data, while the green squares are the FG stars and the cyan squares are the SG stars. The ZAHBs for $Z = 0.0003$ and $Y = 0.25$ (lower line with squares), $Y = 0.35$ (top line) are also shown.

of the pristine gas accretion described by the density $\rho_{0,\text{pr}}$, the time t_{ac} at which the maximum accretion occurs, and by the timescale τ , regulating the width of the gaussian. Another temporal parameter is given by t_{end} , the time at which the simulation ends. Finally, the star formation (SF) efficiency is regulated by the parameter ν (see Eq. 5 in D2010) with values in the range $0 < \nu < 1$. A further parameter is also present: the ratio $x = \rho_{*,\text{SG}}/\rho_{*,\text{tot}}$ between the nowadays alive SG and total (SG+FG) stars; however, this parameter does not enter directly into the model, but is inferred *a posteriori* for a more realistic fit of the data (see below).

The models presented here are aimed at reproducing the $N(Y)$ distributions shown in Fig. 6 (corresponding to the models 4 (F2), 5 (F3) and 6 (F5) of Table 2). Figure 6 shows the $N(Y)$ obtained by three chemical models of F2, F3 and F5, characterized by the following parameters: $(t_{\text{ac},7}, t_{\text{end},7}, \tau_7, \rho_{\text{FG}}, \rho_{0,\text{pr}}, \nu, x) = (5, 9, 0.4, 80, 0.14, 0.08, 0.58)$, $(t_{\text{ac},7}, t_{\text{end},7}, \tau_7, \rho_{\text{FG}}, \rho_{0,\text{pr}}, \nu, x) = (4.5, 8.5, 0.2, 300, 0.1, 0.2, 0.52)$, and $(t_{\text{ac},7}, t_{\text{end},7}, \tau_7, \rho_{\text{FG}}, \rho_{0,\text{pr}}, \nu, x) = (48.5, 9, 0.7, 85, 0.1, 0.13, 0.65)$, respectively; here the times are expressed in 10^7 yr, ρ_{FG} in $M_\odot \text{pc}^{-3}$ and $\rho_{0,\text{pr}}$ is normalized to ρ_{FG} . We stress that the adopted values of x are not arbitrary, but are obtained from the models 4, 5 and 6 (see Table 2). The lower panels in Figure 6 also show the time evolution of the amount of AGB ejecta, pristine gas and SG stellar mass given by the one-zone models. The SG formation starts at an age of 44 Myr, at which the Type II supernova epoch ends in the adopted models by Ventura et al. (2013) of $Z = 0.0003$, and the cooling flow begins to collect the super-AGB ejecta in the cluster core.

The total initial mass of SG stars formed and the ratio of this mass to the initial FG mass in the models that can reproduce the $N(Y)$ in the three clusters can be estimated by looking at the final values of the dashed curves in the

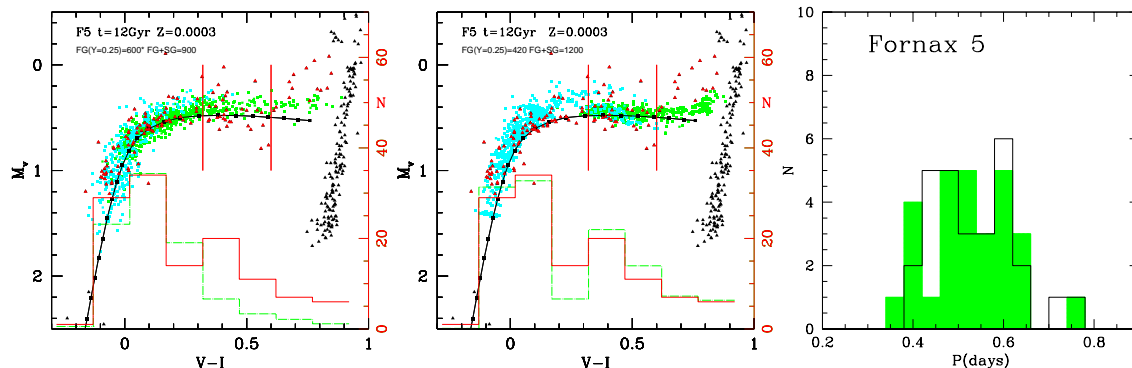


Figure 4. The left panel shows the result of the simulation model 3 of Table 2, where the SG is kept to a minimum; the central panel shows the more satisfactory model 6, and the right panel the observed period distribution from Greco et al. (2009) in the full histogram, compared with the period distribution of a simulation having the inputs of model 6, but for ten times less stars. The left and central panel coding is the same as in Figure 3.

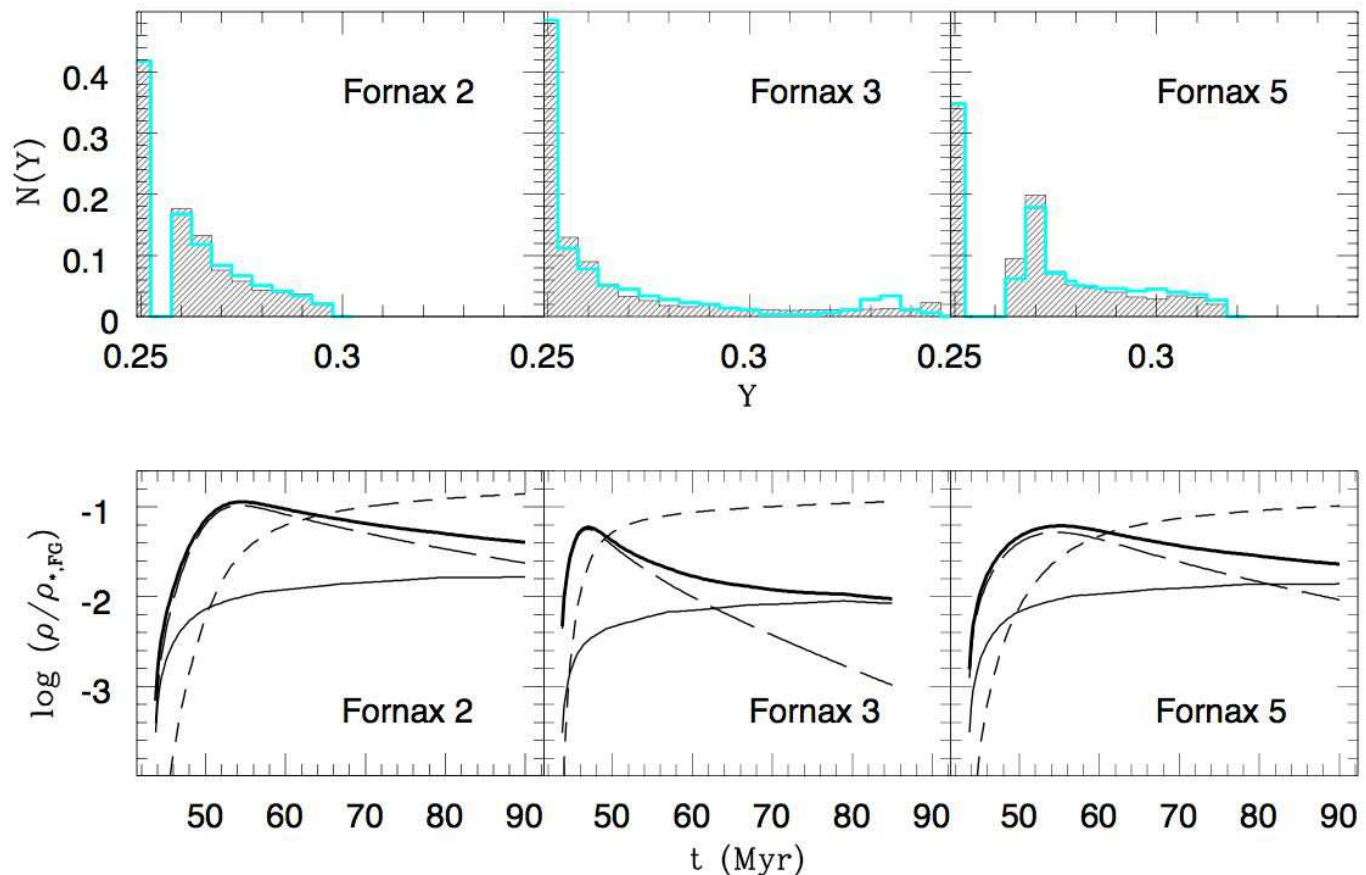


Figure 6. The upper panels show the helium distributions of the three clusters F2, F3 and F5 obtained from the HB morphology (cyan, solid line histograms) and from one-zone chemical models (shaded histograms). The lower panels illustrate the time evolution of different quantities given by the one-zone models: total amount of gas (thick solid line), stellar ejecta (thin solid line), pristine gas (long-dashed line), SG stars (dashed line).

lower panels of Fig. 6. These values along with the current observed fraction of SG stars allow to estimate the ratio the total initial to current GC mass. The estimate will also depend, of course, on the fraction of the initial SG stars still alive.

From Table 2 we have the fraction of SG stars derived from the HB simulations. Although the observed ratio can be dependent on the detail of the dynamical mixing suffered by the two populations, and thus on the location of photometric sample in the clusters (Vesperini et al. 2013), we take it as

a proxy of the fraction of SG mass alive today, with respect to the total GC mass alive today.

$$\frac{N_{\text{SG}}}{N_{\text{tot}}} = \frac{M_{\text{SG alive, now}}}{M_{\text{GC alive, now}}} \quad (5)$$

We choose $0.1M_{\odot}$ as minimum mass entering in the initial mass function, and consider as “alive” the stars between 0.1 and $0.8M_{\odot}$, both for the FG and SG. Throughout this discussion, we apply the stellar mass function by Kroupa 2001.

The cumulative mass of the SG in units of the initial (FG only) mass is shown in Fig. 6. Its final value in the models reproducing the helium distribution of the three cluster is ~ 0.1 in the three successful simulations. Therefore we have:

$$M_{\text{FG}} \simeq 10M_{\text{SG}}. \quad (6)$$

While for M_{FG} entering the chemical evolution models we made the hypothesis that it was initially distributed in stars from 0.1 to $100M_{\odot}$, we still have to consider the mass function of the SG stars. The possible formation of stars in a cooling flow, and the shape of their IMF, is a long-standing problem linked to the more general conundrum of the final physical disposition of the cooled gas. Formation of only low mass stars has been suggested in order to explain the absence of the huge amounts of cold gas expected at the centre of the cooling flows. Currently, there is no conclusive evidence either for or against such an hypothesis (see, e.g. Kroupa & Gilmore 1994, Mathews & Brighenti 1999 and references therein). In the context of the formation of SG stars in GCs, some works (Prantzos & Charbonnel 2006; D’Ercole et al. 2008) have considered that only low mass stars are formed from the SG gas, from 0.1 to $0.8M_{\odot}$. This assumption minimizes the requirements on the initial FG mass, as all the SG mass would still be in stars alive today. A constraint on the SG mass function comes from the assumed AGB scenario: the forming SG stars should not more massive than the minimum mass for supernova explosion, say $8M_{\odot}$, otherwise the stellar explosions would blow out the AGB ejecta, preventing its accumulation within the cluster and any further star formation (e.g. D2012). In this case, only 50% of the mass is today contained in alive stars between 0.1 and $0.8M_{\odot}$.

So we have $M_{\text{SG}} = q \times M_{\text{SG alive, now}}$, with q in the range 1–2.

We are interested in the ratio of the initial GC mass (M_{FG} in equation 6) with respect to the present cluster mass $M_{\text{GC, now}}$. We can write then

$$\frac{M_{\text{FG}}}{M_{\text{GC, now}}} \simeq 10 \times q \times \frac{M_{\text{SG alive, now}}}{M_{\text{GC alive, now}}} \times \frac{M_{\text{GC alive, now}}}{M_{\text{GC, now}}}, \quad (7)$$

From Kroupa (2001), the alive stars constitute a fraction ≈ 0.7 of all the initial stars; this fraction can actually be lower since dynamical evolution and mass loss due to two-body relaxation may reduce this ratio due to the preferential loss of low-mass main sequence stars (see e.g. Vesperini & Heggie 1997, Giersz 2001, Baumgardt & Makino 2003). Substituting in equation 7 the values of $\frac{M_{\text{SG alive, now}}}{M_{\text{GC alive, now}}}$ from Table 2, we get that the initial mass of the clusters were about $q \times 3.5 - 5$ times larger than their current mass. If only half of the initial SG stars are still alive ($q=2$) the initial mass of the clusters must have been about 7–10 times larger than the current mass. We emphasize that different

models (see the example Fornax 2a in the Appendix) indicate that such a factor is not affected by the value of the SF efficiency ν ; in fact, this value is regulated by the need to reproduce the helium distribution, but it is not important in the determination of the final mass of the SG population whenever the replenishing timescale of the accreting gas (AGB ejecta and pristine gas) is shorter than the cluster evolution time (D’Ercole et al. 2008), as indeed is the case in the present models. On the other hand, in the absence of further observational constraint (such as, for example, a well definite O-Na anticorrelation), different set of parameters in the chemical evolution models can give similar, reasonable fit of the helium distributions. In particular, models exist with a shorter evolutive time which give rise to $N(Y)$ close to those shown in Fig. 6; although rather extreme, these models keep open the option of a ratio $\frac{M_{\text{FG initial}}}{M_{\text{GC now}}}$ as high as $\sim 20 - 25$ (see the Appendix). Reversely, we can not increase the mass of the SG by extending the star formation beyond 90–100 Myr, as, at later times, we expect that the onset of type I supernova explosions stops the cooling flow, and, further, the composition of AGB ejecta becomes incompatible with the chemical patterns seen in the GCs of our Galaxy (D’Ercole et al. 2008). We conclude that the initial mass of the clusters F2, F3 and F5 in Fornax is contained within a factor 7–10 of the present masses.

This value is not very different from what we envisaged in D’Ercole et al. (2008), and more explicitly modeled in Vesperini et al. (2010).

A combination of different model ingredients (much narrower range of FG star masses contributing to the gas for SG formation, a shorter duration of the SG formation episode, use of only a small fraction of the polluted gas, lack of pristine gas) may result in the much larger mass factors cited in the literature and discussed in the Introduction.

6 DISCUSSION

There are some critical points in the interpretation of these extra-Galactic GCs that deserve discussion.

This investigation was prompted by the constraint on the possible initial mass of GCs set by Larsen et al. (2012a) on the basis of the observed number of very metal poor field stars in Fornax. As pointed out by Larsen et al. (2012a), the currently known number of very metal poor field stars in Fornax appears to limit the initial mass of GCs in Fornax to be at most 5-6 times its current mass. Interestingly, their analysis also suggests that the initial Fornax cluster system could not include any additional clusters that have now completely dissolved.

Our simulations of the HBs of Fornax clusters suggest that one of them (F1) hosts only the FG component; the lack of SG stars implies that no constraints on its initial mass can be set on the basis of the SG formation and dynamical evolution history. The cluster F4 instead is assigned by recent determinations to a metallicity range ($[\text{Fe}/\text{H}] \sim -1.4$) where stars in Fornax field are in large number, and no strong limit on F4 initial mass is imposed by field stars.

However, the other three clusters (F2, F3, F5: all very metal poor) harbour a substantial SG population. Our models show that an initial mass 4–5 times the present mass is possible, if we impose that all SG stars are alive today. By

adopting an initial mass function of the SG stars extended up to $\sim 8 M_{\odot}$, this estimate must be raised by a factor ~ 2 . A further factor 2.5 is necessary if the time of formation of the SG is shorter than that of the one-zone models shown in Fig. 6. We consider a factor of about 25 as an upper limit.

Although our lower limits are consistent with the constraint set by the study of Larsen et al. (2012a), it is important to understand how robust such a constraint is.

One possible major issue in using the field stars to constrain the birth mass of GCs resides in the estimate of the metallicity of field stars and of GCs.

In this regard, we stress again the impossibility of fitting an isochrone of the appropriate age to a Fornax cluster with $[\text{Fe}/\text{H}] \sim -2.5$ dex: this estimate should be raised at least to -2.3 or -2.2 , depending on the solar metallicity. On the contrary, the CM diagram morphology of cluster F4 does not appear compatible with the factor 10 increase in $[\text{Fe}/\text{H}]$ with respect to F1, reported by recent spectroscopic determinations (see Fig. 2).

As for field metallicity, it is based on Ca-triplet calibration which implies errors of at least 0.1 – 0.2 dex (Battaglia et al. 2008; Starkenburg et al. 2010); besides, the data for Fornax field contain only three stars with $[\text{Fe}/\text{H}] < -1.00$, of which *one* has $[\text{Fe}/\text{H}] < -2.00$, making a reliable calibration difficult. This lack of data for the very metal poor component may arise from a real scarcity, or, as suggested by Starkenburg et al. (2010), from the very small fraction of field RGs sampled at present. They remark also that the very low metallicity tail of Fornax is different both in shape and number from the other classical dSphs and the halo, and comment that the dominant young, metal rich population may well be hiding the scarce metal poor component.

In closing we point out that the use of field stars to constrain the initial GC masses is strongly undermined if Fornax has lost a fraction of its field stars and/or if its globular clusters formed in a different system and were later accreted in Fornax (see Larsen et al. 2012 and references therein).

6.1 A difference in mass loss on the RGB for the FG and SG components?

A difficulty was met when considering the blue side of the HBs in F2, F3 and F5. As an example, we shall consider F3: its “blue” population can not be imputed only to an increased helium. The location of the “zero age” HB would follow the green line in Fig. 7, if we do not allow for an extra mass loss during the RGB evolution of the SG population. A simulation taking into account only the effect of helium variation in decreasing the evolving mass would follow the green line, and would predict a distribution of stars along and above it, while the region between it and the $Y=0.25$ ZAHB is well populated. The blue line shows the ZAHB obtained taking into account an extra-mass loss of $0.03 M_{\odot}$: this is enough to shift the ZAHB to a location much closer to the lower envelope of the data.

A similar situation is found in very metal poor Galactic GCs with a similar distribution of HB stars, including a well populated red, variable and blue regions. As mentioned in D’Antona & Caloi (2008), the RR Lyraes and the red HB of M 68 can be nicely fit by a FG with a small mass spread, as found in the case of M 3 (Caloi & D’Antona 2005). On the

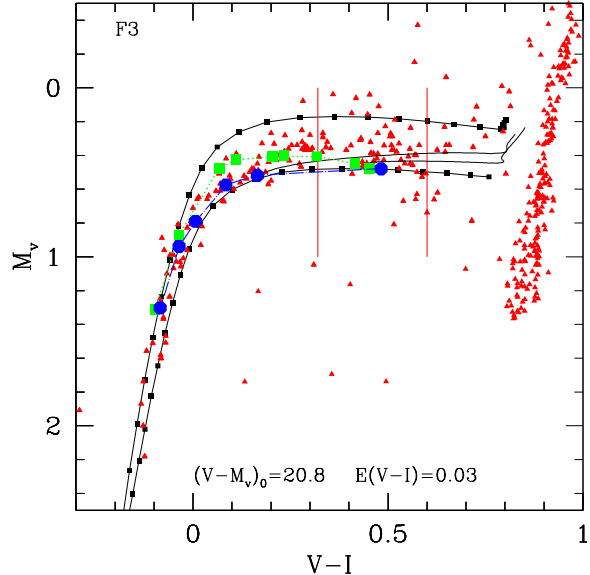


Figure 7. Data for F3 are shown as red triangles. Green squares indicate the ZAHB with enhanced Y assuming the same mass loss as for $Y=0.25$. An extra mass loss of $0.03 M_{\odot}$ gives rise to the ZAHB indicated by blue circles, much closer to the observations. The ZAHBs for $Y=0.25$ and $Y=0.35$ are also shown.

contrary, the simulated luminosity of the blue side results too large if interpreted only in terms of an increased helium content. The same considerations apply to the HB in M15, another very metal poor GC rich in blue, variable and red HB stars.

This difficulty is less evident in the case of the more metal rich ($Z \sim 10^{-3}$) Galactic GCs analysed up to now, but hints that a larger mass loss is required for the SG come from NGC 1851 (Salaris et al. 2008) and from the analysis by Dalessandro et al. (2013) of the HBs in M 3, M 13 and M 79.

An increase in mass loss from SG giants may be related to an average larger angular velocity in SG main sequence stars with respect to FG ones. In current views, SG population takes origin from a cooling flow collecting at the cluster centre and so the initial number density of SG MS stars is larger than in the FG case. We may speculate that such an increased density favours an increase in the average rotational velocity of the newly formed stars. The effects of an initial, relatively slow angular rotation in Pop II main sequence stars (ω_{MS}) has been studied, in first approximation, in the years ’70s by Mengel & Gross (1976) and Renzini (1977). The result was that, as long as ω_{MS} does not exceed $2 \cdot 10^{-4} \text{ s}^{-1}$, the turnoff age is not altered, while both the luminosity at the He-flash and the He-core mass increase (eqs. 2.19 and 2.20 in Renzini’s paper). On the basis of Fusi-Pecci & Renzini (1975) treatment of mass loss along the RG branch, Renzini gives an estimate of the relation between the increase in luminosity at the RG tip and the related increase in mass loss. A mass loss increase of $0.03 M_{\odot}$ requires an increase in $\log(L/L_{\odot})$ at the RG tip of 0.01, in turn requiring an ω_{MS} of about $1.2 \cdot 10^{-4} \text{ s}^{-1}$. The expected increase in the core mass is $0.004 M_{\odot}$. Such an increase does not affect substantially the ZAHB loca-

tion, whose luminosity would be *larger* by only ~ 0.03 mag.⁴ The constancy of the assumed mass loss increase for the SG population implies a small dispersion in ω_{MS} , an approximation in line with the qualitative treatment exposed here. We stress that the hypothesis of an increased average rotation is just a suggestion, in view of future investigations on the subject.

A final remark on the stellar components of Fornax field. According to our interpretation of the HBs, at least three GCs (F2, F3 and F5) host a large population of SG stars, mostly located on the blue side of the HB. From the exemplifications of Figs. 3 (left panel), 4 (central panel) and 5, we qualitatively see that the FG stars do not extend much to the blue side of the RR Lyr gap (in the cases displayed, there are no FG stars in the HB at $(V-I)_0 \lesssim 0.3$). If our interpretation of the HB morphology is correct, it seems therefore that these objects can form *only* in the environment of a GC, from which they populate the galactic field when they are lost by the native cluster. As discussed in Vesperini et al. (2013), SG star evaporation from GCs into the host galaxy field would occur during a cluster long-term evolution driven by two-body relaxation.

We analyzed the data in de Boer et al. (2012), who present deep optical photometry of the Fornax dSph in the B, V and I filters obtained using the CTIO 4-m MOSAIC II camera. They define an elliptical radius r_{ell} to provide a distance measurement from the center. Since the spatial coverage of the B and V filters is complete for $r_{\text{ell}} \lesssim 0.8$ degrees, while the I filters is complete for $r_{\text{ell}} \lesssim 0.4$ degrees we have used B and V bands data with $0.5 < r_{\text{ell}} < 0.8$ in order to be able to isolate mostly the old population. In fact de Boer et al. 2012 have shown that the young and intermediate age stars are more centrally concentrated than the old stars. The data we use do not give information on stellar metallicity, but a combination of the spectroscopic catalogs of DART (CaT and HR), the medium resolution spectra catalog by Kirby et al. (2010) (med. res) and the CaT data by Pont et al. (2004), kindly done by K. de Boer (private communication) shows that about half of the stars at $0.5 < r_{\text{ell}} < 0.8$ have metallicity $[\text{Fe}/\text{H}] < -1.4$, while most of the younger stars of $[\text{Fe}/\text{H}] > -1.0$ are confined within $r_{\text{ell}} < 0.4$. We find that this region of Fornax field shows a well populated sample of stars hotter than the blue edge of the RR Lyrae strip (fixed at $(B-V)_0 = 0.2$ mag) and make up 9–11% of the whole HB population (assuming $E(B-V) = 0.03$ mag). If we assume that all the stars having $[\text{Fe}/\text{H}] > -1.4$ populate the red HB only, the percentage of blue HB stars in the low metallicity sample is $\sim 20\%$.

A further detailed analysis of the HB field population would be very important to shed light on the possible connection between multiple stellar populations in globular clusters and in the Fornax field stars.

ACKNOWLEDGMENTS

We thank Thomas de Boer and Eline Tolstoy for sharing their photometry of Fornax field stars. We also thank Gisella

Clementini for useful discussion on the RR Lyrs in the Fornax clusters, and Carlo Corsi for making available the clusters photometric data.

F.D., A.D and P.V. have been supported by the PRIN-INAFA 2011 “Multiple populations in globular clusters: their role in the Galaxy assembly”, P.I. E. Carretta. EV was supported in part by grant NASA-NNX13AF45G.

REFERENCES

- Angulo C., Arnould M., Rayet M., et al. 1999, Nucl. Phys. A, 656, 3
- Asplund, M., Grevesse, N., Sauval, A. J., & Scott, P. 2009, ARA&A, 47, 481
- Bahcall, J. N., Pinsonneault, M. H., & Basu, S. 2001, ApJ, 555, 990
- Bahcall, J. N., Serenelli, A. M., & Pinsonneault, M. 2004, ApJ, 614, 464
- Bahcall, J. N., Basu, S., & Serenelli, A. M. 2005, ApJ, 631, 1281
- Bahcall, J. N., Serenelli, A. M., & Basu, S. 2006, ApJS, 165, 400
- Basu, S., & Antia, H. M. 2004, ApJ, 606, L85
- Battaglia, G., Tolstoy, E., Helmi, A., et al. 2006, A&A, 459, 423
- Battaglia, G., Irwin, M., Tolstoy, E., et al. 2008, MNRAS, 383, 183
- Baumgardt, H., Makino, J., 2003, MNRAS, 340, 227
- Bekki, K., Campbell, S. W., Lattanzio, J. C., & Norris, J. E. 2007, MNRAS, 377, 335
- Bekki, K. 2011, MNRAS, 412, 2241
- Buonanno, R., Corsi, C. E., Zinn, R., et al. 1998, ApJ, 501, L33
- Buonanno, R., Corsi, C. E., Castellani, M., et al. 1999, AJ, 118, 1671
- Caloi, V., & D’Antona, F. 2005, A&A, 435, 987
- Caloi, V., & D’Antona, F. 2008, ApJ, 673, 847
- Caloi, V., & D’Antona, F. 2011, MNRAS, 417, 228
- Carretta, E., & Gratton, R. G. 1997, A&AS, 121, 95
- Carretta, E., et al. 2009a, A&A, 505, 117
- Carretta, E., Bragaglia, A., Gratton, R., D’Orazi, V., & Lucatello, S. 2009b, A&A, 508, 695
- Cassisi, S., Potekhin, A. Y., Pietrinferni, A., Catelan, M., & Salaris, M. 2007, ApJ, 661, 1094
- Christensen-Dalsgaard, J., Dappen, W., Ajukov, S. V., et al. 1996, Science, 272, 1286
- Cole, A. A., Smecker-Hane, T. A., Tolstoy, E., Bosler, T. L., & Gallagher, J. S. 2004, MNRAS, 347, 367
- Da Costa, G. S., & Armandroff, T. E. 1995, AJ, 109, 2533
- Da Costa, G. S., & Hatzidimitriou, D. 1998, AJ, 115, 1934
- Dalessandro, E., Salaris, M., Ferraro, F. R., Mucciarelli, A., & Cassisi, S. 2013, MNRAS, 430, 459
- D’Antona, F., Caloi, V., Montalbán, J., Ventura, P., & Gratton, R. 2002, A&A 395, 69
- D’Antona, F., & Caloi, V. 2008, MNRAS, 390, 693
- de Boer, T. J. L., Tolstoy, E., Hill, V., et al. 2012, A&A, 544, A73
- Decressin, T., Charbonnel, C., & Meynet, G. 2007, A&A, 475, 859
- D’Ercole, A., Vesperini, E., D’Antona, F., McMillan, S. L. W., Recchi, S., 2008, MNRAS, 391, 825

⁴ We use the relation $\frac{\delta \log L/L_{\odot}}{\delta M_{\text{core}}/M_{\odot}} = 3$ from Sweigart & Gross (1976).

- D’Ercole, A., D’Antona, F., Ventura, P., Vesperini, E., & McMillan, S. L. W. 2010, *MNRAS*, 407, 854 (D2010)
- D’Ercole, A., et al. 2012, *MNRAS*, 423, 1521 (D2012)
- Di Criscienzo, M., Marconi, M., & Caputo, F. 2004, *ApJ*, 612, 1092
- Di Criscienzo, M., et al. 2011, *MNRAS*, 414, 3381
- Dotter, A., Chaboyer, B., Jevremović, D., et al. 2007, *AJ*, 134, 376
- Ferguson J. W., Alexander D. R., Allard F. et al., 2005, *ApJ*, 623, 585
- Freeman, K., & Bland-Hawthorn, J. 2002, *ARA&A*, 40, 487
- Fusi-Pecchi, F., & Renzini, A. 1975, *A&A*, 39, 413
- Giersz, M. 2001, *MNRAS*, 324, 218
- Gratton, R. G., Carretta, E., & Bragaglia, A. 2012, *A&A Rev*, 20, 50
- Greco, C., 2007, PhD Thesis, XIX Ciclo, Università di Bologna
- Greco, C., Clementini, G., Catelan, M., et al. 2009, *ApJ*, 701, 1323
- Grevesse N., Sauval A.J, 1998, *SSrv*, 85, 161
- Harris, W. E., & van den Bergh, S. 1981, *AJ*, 86, 1627
- Hodge, P.V. 1961, *AJ*, 66, 83
- Iglesias, C.A., Rogers, F.J., *ApJ*, 464, 943
- Kirby, E. N., Guhathakurta, P., Simon, J. D., et al. 2010, *ApJS*, 191, 352
- Kroupa, P., Tout, C. A., & Gilmore, G. 1993, *MNRAS*, 262, 545
- Kroupa, P. 2001, *MNRAS*, 322, 231
- Kroupa P., & Gilmore G. 1994, *MNRAS*, 269, 655
- Larsen, S. S., Strader, J., & Brodie, J. P. 2012a, *A&A*, 544, L14
- Larsen, S. S., Brodie, J. P., & Strader, J. 2012b, *A&A*, 546, A53
- Letarte, B., Hill, V., Jablonka, P., et al. 2006, *A&A*, 453, 547
- Mackey, A. D., & Gilmore, G. F. 2003, *MNRAS*, 345, 747
- Mathews W. G., & Brighenti F. 1999, *ApJ*, 527, L31
- Mengel, J. G., & Gross, P. G. 1976, *Ap&SS*, 41, 407
- Montalbán, J., Miglio, A., Noels, A., Grevesse, N., & di Mauro, M. P. 2004, *SOHO 14 Helio- and Asteroseismology: Towards a Golden Future*, 559, 574
- Montalban, J., Miglio, A., Theado, S., Noels, A., & Grevesse, N. 2006, *Communications in Asteroseismology*, 147, 80
- Pont, F., Zinn, R., Gallart, C., Hardy, E., & Winnick, R. 2004, *AJ*, 127, 840
- Potekhin, A. Y., Baiko, D. A., Haensel, P., & Yakovlev, D. G. 1999, *A&A*, 346, 345
- Prantzos, N., & Charbonnel, C. 2006, *A&A*, 458, 135
- Reimers, D. 1975, *Problems in stellar atmospheres and envelopes.*, (A75-42151 21-90) New York, Springer-Verlag New York, Inc., 1975, p. 229
- Renzini, A. 1977, in *Advanced Stages in Stellar Evolution*, ed. I. Iben, Jr., A. Renzini, & D. N. Schramm (Heidelberg: Springer)
- Renzini, A. 2008, *MNRAS*, 391, 354
- Renzini, A. 2013, arXiv:1302.0329
- Rutledge, G. A., Hesser, J. E., & Stetson, P. B. 1997, *PASP*, 109, 907
- Salaris, M., Cassisi, S., & Pietrinferni, A. 2008, *ApJ*, 678, L25
- Schaerer, D., & Charbonnel, C. 2011, *MNRAS*, 413, 2297
- Starkenbug, E., Hill, V., Tolstoy, E., et al. 2010, *A&A*, 513, A34
- Strader, J., Brodie, J. P., Forbes, D. A., Beasley, M. A., & Huchra, J. P. 2003, *AJ*, 125, 1291
- Sweigart, A. V., & Gross, P. G. 1976, *ApJS*, 32, 367
- Tolstoy, E., Irwin, M. J., Cole, A. A., et al. 2001, *MNRAS*, 327, 918
- Ventura, P., Di Criscienzo, M., Carini, R., & D’Antona, F. 2013, *MNRAS*, 431, 3642
- Vesperini, E., Heggie, D.C., 1997, *MNRAS*, 289, 898
- Vesperini, E., McMillan, S. L. W., & Portegies Zwart, S. 2009, *ApJ*, 698, 615
- Vesperini, E., McMillan, S. L. W., D’Antona, F., & D’Ercole, A. 2010, *ApJ*, 718, L112
- Vesperini, E., McMillan, S. L. W., D’Antona, F., & D’Ercole, A. 2013, *MNRAS*, 429, 1913

APPENDIX A: CHEMICAL MODEL ANALYSIS

In this Appendix we discuss in a little more in detail the response of our one-zone model to the variation of the SF efficiency ν and to the duration of the evolutive time. In all the models presented in the text (Fig. 6), the SG formation lasts until a total age of 85–90 Myr. As the only constraint is the helium distribution function, this choice is not unique. As an example, Figure A1 shows three different cases for the cluster F2: in the first case (left panel, Fornax 2a) we show that the total amount of gas in SG stars barely increases when we shift from $\nu=0.08$ (standard model for F2, in Fig. 6) to $\nu=1$, because, as discussed by D’Ercole et al. (2008), the accretion time is shorter than the evolutive time. Other models are possible to reproduce $N(Y)$, and the central panel shows an extreme model, with $\nu=1$, in which the star formation lasts for only 8 Myr (Fornax 2b). Obviously, the mass in SG stars is now a much smaller fraction of the FG mass; we have $\rho_{SG} \simeq 0.04\rho_{FG}$, leading to a ratio $FG_{initial}/(FG+SG)_{now} \sim 30$. If we further reduce the star formation efficiency to $\nu=0.1$ (Fornax 2c), the total mass achieved in SG stars is even smaller, because now the accretion time is comparable to the evolution time, and not all the gas collected in the cluster core can be used to form stars in such a short time.

We regard the case Fornax 2b as an extreme example still able to obtain a satisfactory $N(Y)$, but only other information on the chemistry of SG stars can improve the fit with observations and allow us to choose among different models. For now, we use the models of Fig. 6 as standard models for the three clusters.

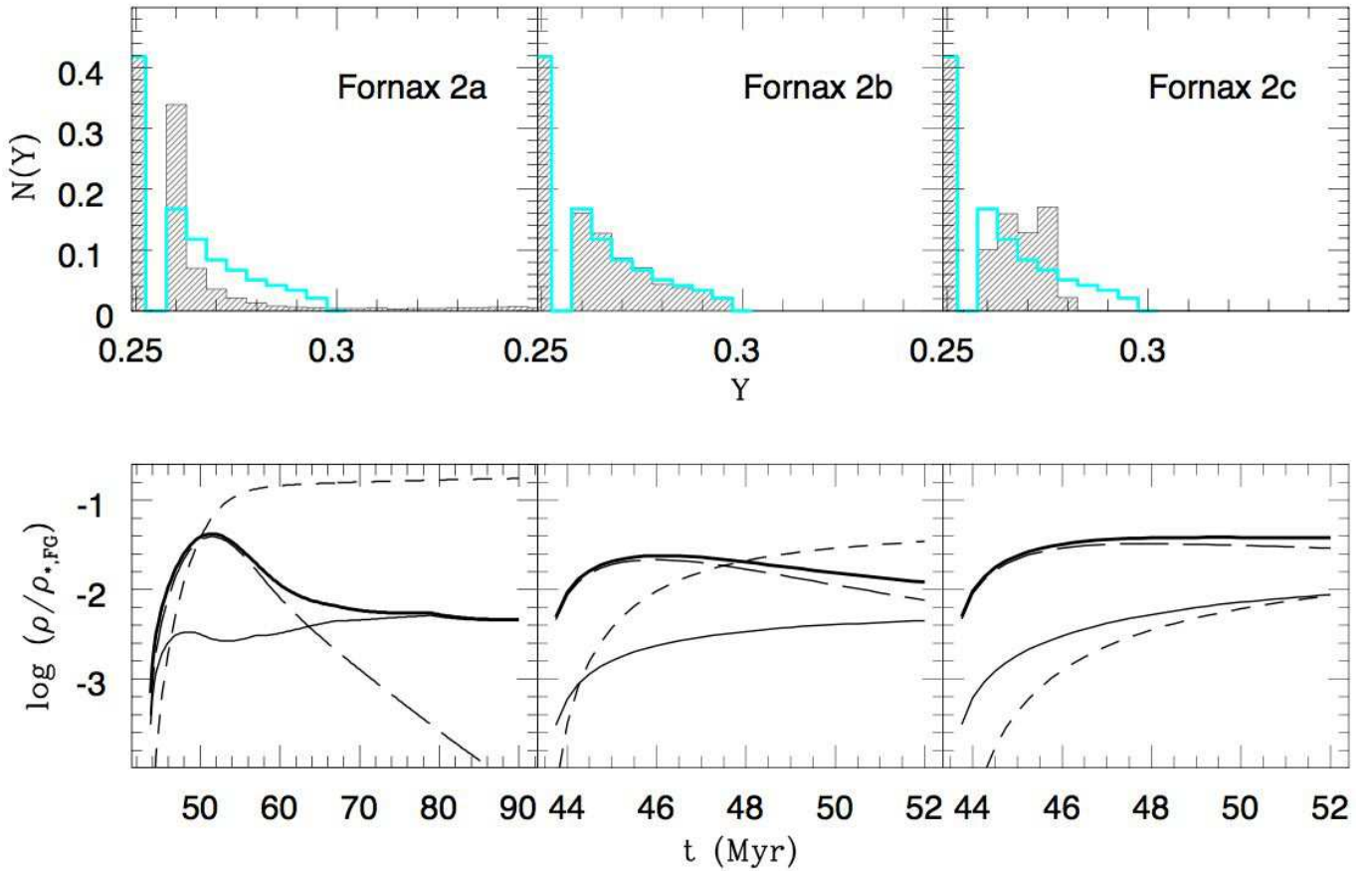


Figure A1. The symbols are the same as for for Fig. 6. The figure shows three cases of chemical evolution for F2. The left panel shows the difference with the standard case, when we assume star formation efficiency $\nu=1$: the helium distribution is different, but the total mass in SG is barely larger than in the standard case having $\nu=1$ because the accretion time is shorter than the evolutionary time. The central panel shows a good reproduction of $N(Y)$ achieved by a model in which the SF formation has a short duration (up to 52 Myr) and $\nu=1$. The right panel shows the result for the same inputs of the central panel, but $\nu=0.1$. In this case, the total amount of gas in SG stars is a factor 2–3 smaller, as the accretion time is now comparable to the evolutionary time.